

ASSESSING THE BLANK CARBON CONTRIBUTION, ISOTOPE MASS BALANCE, AND KINETIC ISOTOPE FRACTIONATION OF THE RAMPED PYROLYSIS/OXIDATION INSTRUMENT AT NOSAMS

Jordon D Hemingway^{1,2*} • Valier V Galy¹ • Alan R Gagnon³ • Katherine E Grant⁴ • Sarah Z Rosengard^{1,2} • Guillaume Soulet^{3†} • Prosper K Zigah³ • Ann P McNichol³

¹Department of Marine Chemistry and Geochemistry, Woods Hole Oceanographic Institution, 266 Woods Hole Road, Woods Hole, MA 02543, USA.

²Massachusetts Institute of Technology – Woods Hole Oceanographic Institution Joint Program in Oceanography and Applied Ocean Science and Engineering, 77 Massachusetts Avenue, Cambridge, MA 02139, USA.

³Department of Geology and Geophysics, Woods Hole Oceanographic Institution, 266 Woods Hole Road, Woods Hole, MA 02543, USA.

⁴Department of Earth and Atmospheric Sciences, Cornell University, Ithaca, NY 14853, USA.

ABSTRACT. We estimate the blank carbon mass over the course of a typical Ramped PyrOx (RPO) analysis (150–1000°C; 5°C × min⁻¹) to be (3.7 ± 0.6) μg C with an Fm value of 0.555 ± 0.042 and a δ¹³C value of (−29.0 ± 0.1) ‰ VPDB. Additionally, we provide equations for RPO Fm and δ¹³C blank corrections, including associated error propagation. By comparing RPO mass-weighted mean and independently measured bulk δ¹³C values for a compilation of environmental samples and standard reference materials (SRMs), we observe a small yet consistent ¹³C depletion within the RPO instrument (mean–bulk: μ = −0.8‰; ±1σ = 0.9‰; n = 66). In contrast, because they are fractionation-corrected by definition, mass-weighted mean Fm values accurately match bulk measurements (mean–bulk: μ = 0.005; ±1σ = 0.014; n = 36). Lastly, we show there exists no significant intra-sample δ¹³C variability across carbonate SRM peaks, indicating minimal mass-dependent kinetic isotope fractionation during RPO analysis. These data are best explained by a difference in activation energy between ¹³C- and ¹²C-containing compounds (¹³–¹²ΔE) of 0.3–1.8 J × mol⁻¹, indicating that blank and mass-balance corrected RPO δ¹³C values accurately retain carbon source isotope signals to within 1–2‰.

KEYWORDS: Ramped PyrOx, blank assessment, kinetic fractionation.

INTRODUCTION

Thermoanalytical instruments such as thermogravimetry (TG) and pyrolysis gas chromatography (pyGC) are frequently used in petroleum geoscience (Peters 1986), biofuels research (White et al. 2011), and soil science (Plante et al. 2009) to monitor the thermal reactivity of organic carbon (OC) contained within environmental samples. Additionally, petroleum geochemists have long coupled thermal analysis methods with isotope ratio measurements in order to investigate the origins and maturity of thermogenic hydrocarbons, leading to the development of techniques such as pyGC-isotope ratio mass spectrometry (IRMS; Galimov 1988; Berner and Faber 1996; Cramer 2004). However, despite their potential to probe the relationship between OC molecular composition, isotope composition, and thermal reactivity, coupled thermal-isotope methods have found limited use in other fields of organic geochemistry. Still, preliminary studies analyzing environmental samples indicate that TG coupled with IRMS can yield meaningful trends in stable-carbon isotope (¹²C, ¹³C) composition with temperature (Lopez-Capel et al. 2006; Lopez-Capel et al. 2008). Furthermore, Szidat et al. (2004) and Currie and Kessler (2005) successfully separated and determined the radiocarbon (¹⁴C) content of organic and elemental (“black”) carbon fractions in aerosols using a stepped-temperature approach, confirming the possibility that thermal-isotope techniques can be used in tandem with ¹⁴C analysis.

Recently, a novel instrument has been developed at the National Ocean Sciences Accelerator Mass Spectrometry (NOSAMS) facility to determine both the stable and ¹⁴C isotope composition of evolved gases from environmental samples with increasing temperature

*Corresponding author. Email: jhemingway@whoi.edu.

†Current address: Department of Geography, Durham University, South Road, Durham DH1 3LE, UK

(Rosenheim et al. 2008). This method, termed Ramped PyrOx or RPO, is increasingly being utilized in a host of environments in order to understand the relationship between carbon source, ^{14}C content, and thermal reactivity (e.g. Rosenheim and Galy 2012; Plante et al. 2013; Rosenheim et al. 2013b; Schreiner et al. 2014; Bianchi et al. 2015). However, a complete understanding of isotope fractionation within the RPO instrument is currently lacking, hindering our ability to accurately interpret evolved-gas ^{13}C composition as a carbon source tracer. Additionally, RPO analysis shows promise for improving age-model constraints on carbonate-free sediments (Rosenheim et al. 2013a; Subt et al. 2016), although this application requires that contaminant (“blank”) carbon contributions and ^{14}C mass balance are well constrained. Therefore, the aim of this study is to investigate the blank carbon contribution, isotope mass balance, and kinetic fractionation within the RPO instrument located at NOSAMS.

ANALYTICAL SETUP

The NOSAMS RPO instrumental design is originally described in Rosenheim et al. (2008) and has since been modified to lower contaminant carbon inputs by replacing all plumbing with copper tubing, improve gas flow rates, and improve temperature ramp stability (Plante et al. 2013). In this setup, ultra-high purity (UHP) He gas flows at $32\text{ mL} \times \text{min}^{-1}$ into a precombusted (850°C , 5 hr) quartz reactor sitting in a two-stage oven containing sample material to be pyrolyzed/oxidized (Figure 1 a,b). He gas is combined with $3\text{ mL} \times \text{min}^{-1}$ UHP

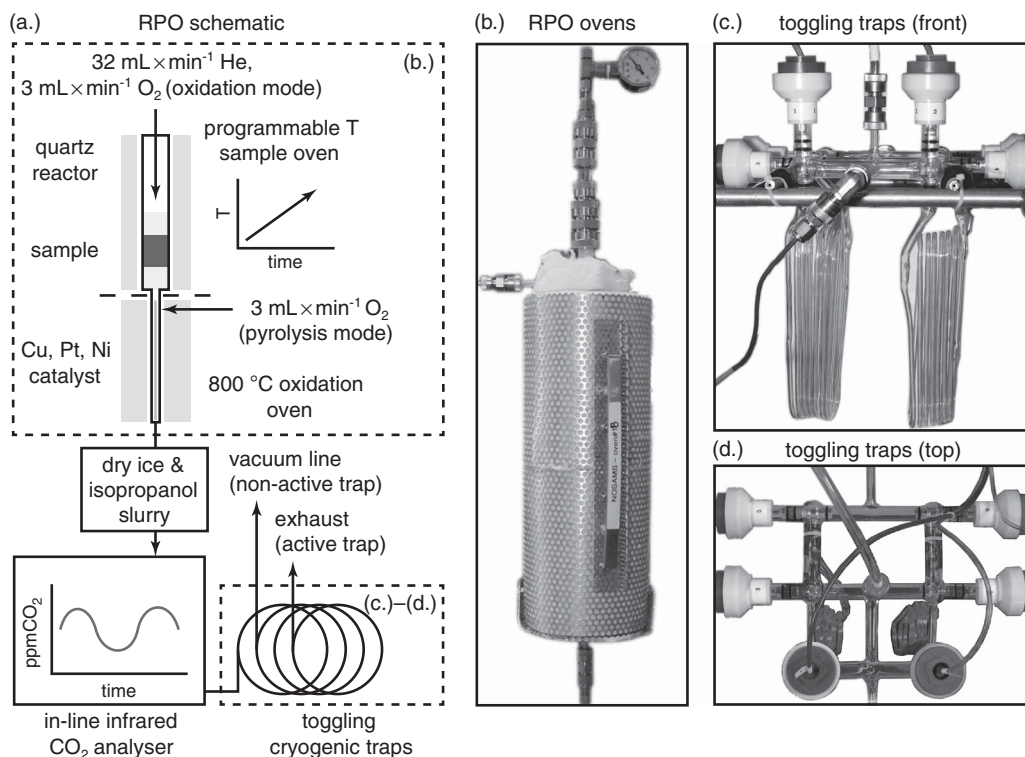


Figure 1 The NOSAMS RPO instrumental setup: (a.) schematic diagram, (b.) photo of the ovens, and (c.)–(d.) photos of the toggling trap apparatus. Dashed boxes in panel (a.) indicate the regions shown in panels (b.)–(d.).

O₂ either (1) prior to entering the quartz reactor (“oxidation mode”) or (2) downstream of sample material but upstream of a Cu, Pt, and Ni wire catalyst via a reactor side-arm (“pyrolysis mode”). An optimized, combined flow rate of 35 mL × min⁻¹ was chosen to minimize transfer time within the system while still allowing sufficient contact time with the wire catalyst and complete cryogenic trapping of CO₂. During analysis, the lower oven containing the catalyst is held at 800°C to facilitate oxidation of reduced carbon-containing gases to CO₂, while the upper oven containing the sample is ramped at a user-defined rate with ≈5% precision [typically (5 ± 0.2) °C × min⁻¹]. We note that care must be taken when analyzing HCl-fumigated soil/sediment samples (e.g. Plante et al. 2013) as well as marine sediments and dissolved OC, as residual chloride has been observed to interact with and melt the catalysis wire, thus blocking gas flow within the reactor.

After exiting the ovens, water vapor is removed using a dry ice and isopropanol slurry. Gases are then passed into an in-line Sable Systems[®] CA-10 infrared gas analyzer (IRGA) where CO₂ concentration (in parts per million by volume, ppm CO₂) is measured photometrically at 1-s resolution with ≈5 ppm CO₂ precision in order to generate a plot of temperature versus CO₂ concentration (termed a thermogram). Finally, gases are transferred to a toggling trap apparatus (Figure 1 a,c,d) in which CO₂ is frozen using liquid N₂ while He and O₂ are vented to the atmosphere. At user-defined temperatures, the collecting trap is toggled and CO₂ for each temperature window (termed a fraction) is transferred to a vacuum line, quantified manometrically, and sealed into a precombusted (525°C, 1 hr) 6 mm Pyrex[®] tube containing 100 mg CuO and 10 mg Ag pellets. Following each analysis, tubes are recombusted (525°C, 1 hr) to remove sulfur-containing contaminant gases and CO₂ carbon isotopes are measured following standard NOSAMS procedures (McNichol et al. 1992, 1994a; Pearson et al. 1998). Between each analysis, CO₂ concentration measurements are calibrated using a 2-point calibration curve by plumbing (1) UHP He, and (2) UHP He containing a known CO₂ concentration directly through the IRGA.

RESULTS AND DISCUSSION

NOSAMS RPO Blank Correction

In order to estimate the RPO blank carbon mass and isotope composition, we directly trapped and analyzed CO₂ evolved from empty, precombusted reactor inserts over the typical analytical temperature range (150–1000°C). Although blank carbon contribution is often determined by monitoring deflections from accepted standard reference material (SRM) isotope compositions (i.e. isotope dilution and “modern-dead” methods; Pearson et al. 1998; Santos et al. 2007; Fernandez et al. 2014; Shah Walter et al. 2015), the direct measurement method employed here is better-suited for the RPO instrument for the following reasons:

1. Deflections from accepted SRM isotope values are only informative over the narrow temperature range in which the material decomposes, rather than over the course of an entire analysis;
2. For stable isotopes, it is possible that kinetic fractionation could overprint isotope deflections due to blank carbon contribution (e.g. Cramer 2004; Dieckmann 2005); and
3. Isotope deflection methods are unable to separate blank carbon contributed within the quartz reactor (i.e. time-dependent blank carbon; Fernandez et al. 2014) from that contributed when switching the toggling trap apparatus (i.e. time-independent blank carbon; Fernandez et al. 2014).

Table 1 NOSAMS RPO blank carbon mass, flux, and isotope composition. For measurements with $n = 1$, reported std. dev. is instrumental uncertainty. For measurements with $n = 2$, reported std. dev. is $\frac{1}{2}$ of the range between values.

Toggles	Mass ($\mu\text{g C}$)			Flux ($\text{ng C} \times ^\circ\text{C}^{-1}$)			$\delta^{13}\text{C}$ (‰ VPDB)			Fm		
	Mean	Std. dev.	n	Mean	Std. dev.	n	Mean	Std. dev.	n	Mean	Std. dev.	n
0	4.0	0.8	4	4.7	0.9	4	-29.0	0.1	1	0.558	0.010	1
2	3.6	0.0	2	4.6	0.0	2	—	—	—	0.595	0.012	1
5	3.4	0.3	2	4.0	0.4	2	—	—	—	0.512	0.013	1
Mean	3.7	0.6	8	4.5	0.7	8	-29.0	0.1	1	0.555	0.042	3

To address point (3), we calculated the blank carbon mass and ^{14}C content when the traps were toggled 0, 2, and 5 times at evenly spaced intervals during CO_2 collection between 150 and 1000°C (leading to 1, 3, and 6 collected fractions, respectively). For 2- and 5-toggle experiments, individual fractions were recombined within the vacuum line before transferring to a 6 mm Pyrex tube to keep subsequent steps identical across all experimental conditions. Each experiment was performed in duplicate and the CO_2 mass from each analysis was quantified separately before pairs were combined for ultra-small ^{14}C analysis (Shah Walter et al. 2015). Results are corrected for the $^{13}\text{C}/^{12}\text{C}$ ratio as measured on the AMS (Santos et al. 2007) and are reported in Fm notation following Stuiver and Polach (1977). We note that Fm reported here is identical to the “ $^{14}\text{a}_\text{N}$ ” notation of Mook and van der Plicht (1999) as well as the “ F^{14}C ” notation of Reimer et al. (2004). The 0-toggle experiment was repeated in duplicate for ^{13}C analysis using a dual-inlet IRMS as described in McNichol et al. (1994a), and $^{13}\text{C}/^{12}\text{C}$ ratios are reported in $\delta^{13}\text{C}$ notation (‰ relative to Vienna Pee Dee Belemnite, or VPDB).

Resulting blank carbon mass is independent of the number of toggles throughout the analysis (Table 1), averaging $(3.7 \pm 0.6) \mu\text{g C}$ ($n = 8$) and indicating that the act of toggling the traps contributes a negligible amount of time-independent blank carbon. This is further supported by the near-identical Fm values across experimental conditions (Table 1). We therefore combine measurements from all experiments and calculate an average blank carbon Fm value of 0.555 ± 0.042 ($n = 3$). Because both mass and Fm values are nearly identical across all experiments, we apply the measured 0-toggle blank carbon $\delta^{13}\text{C}$ value of $(-29.0 \pm 0.1) \text{‰ VPDB}$ (Table 1) regardless of the number of toggles.

Blank carbon mass calculated here is significantly lower and less variable than that determined for a similar RPO system [c.f. $(12.9 \pm 7.0) \mu\text{g C}$; Fernandez et al. 2014], likely due to recent valve and plumbing upgrades on the NOSAMS instrument (Plante et al. 2013). Additionally, photometric measurements suggest that time-dependent blank carbon contribution is not concentrated within any particular temperature range—that is, there exist no distinct peaks within the blank thermograms (Figure 2). Although the mean blank flux appears to drop slightly from $(5.8 \pm 0.7) \text{ng C} \times ^\circ\text{C}^{-1}$ when $T < 550^\circ\text{C}$ to $(3.1 \pm 1.0) \text{ng C} \times ^\circ\text{C}^{-1}$ when $T \geq 550^\circ\text{C}$, it can nonetheless be reasonably described as constant throughout the analysis within the 95% confidence interval of the manometric measurements (Figure 2).

Dividing the manometric blank carbon mass by the experimental temperature range results in a blank carbon flux of $(4.5 \pm 0.7) \text{ng C} \times ^\circ\text{C}^{-1}$ (assuming a $5^\circ\text{C} \times \text{min}^{-1}$ ramp rate; Table 1). We therefore correct the mass of carbon in each RPO fraction for blank contribution according to

$$m_s = m_m - \phi_b \Delta T \quad (1)$$

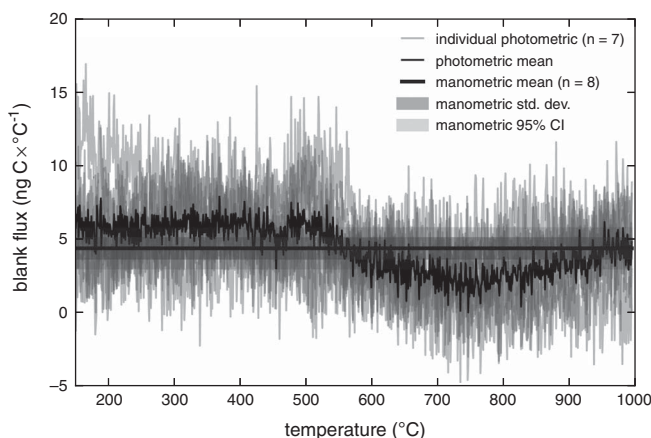


Figure 2 RPO blank carbon flux for a ramp rate of $5^{\circ}\text{C} \times \text{min}^{-1}$ as determined photometrically and manometrically. For photometric measurements, absolute CO_2 concentrations were normalized such that the mean value for each analysis is equal to the manometric mean, as small differences in IRGA baseline calibration between analyses leads to large changes in calculated blank flux.

where m_s is the true sample carbon mass, m_m is the measured carbon mass, ϕ_b is the blank carbon flux (in units of $\text{mass} \times ^{\circ}\text{C}^{-1}$), and ΔT is the temperature range over which the CO_2 was collected. Here, we proceed using the manometric average ϕ_b value of $(4.5 \pm 0.7) \text{ ng C} \times ^{\circ}\text{C}^{-1}$. However, we note that temperature-specific ϕ_b values listed above could offer slight improvements in blank-corrected mass accuracy, although these results will typically be statistically identical to those using the manometric average value. Additionally, we propagate uncertainty for this correction according to

$$\sigma_{m_s} = \sqrt{(\sigma_{m_m})^2 + (\sigma_{\phi_b} \Delta T)^2} \quad (2)$$

where σ is the standard deviation associated with each subscripted measurement. This assumes that ΔT is known perfectly (i.e. $\sigma_{\Delta T} \equiv 0.0$) and that the uncertainty in m_m and ϕ_b are uncorrelated, which is reasonable given that $m_s \approx m_m \gg \Delta T \phi_b$. Similarly, we treat the measured CO_2 isotope composition as a weighted average of sample carbon and blank carbon, and correct for blank contribution following

$${}^x\text{R}_s = \frac{m_m {}^x\text{R}_m - \phi_b \Delta T {}^x\text{R}_b}{m_s} \quad (3)$$

where ${}^x\text{R}_i$ is the ${}^x\text{C}/^{12}\text{C}$ isotope ratio of component i [$x = 13, 14$; $i = (\text{s})\text{ample}, (\text{m})\text{easured}, (\text{b})\text{lank}$], with ${}^{13}\text{R}_i$ expressed in $\delta^{13}\text{C}$ notation (‰ VPDB) and ${}^{14}\text{R}_i$ expressed in Fm notation. Lastly, we propagate uncertainty associated with isotope corrections. Because $m_s \approx m_m$, we cancel these where appropriate to avoid large covariance terms, leading to

$$\sigma_{{}^x\text{R}_s} \cong \sqrt{(\sigma_{{}^x\text{R}_m})^2 + \left(\frac{\Delta T {}^x\text{R}_b}{m_s} \sigma_{\phi_b}\right)^2 + \left(\frac{\phi_b \Delta T}{m_s} \sigma_{{}^x\text{R}_b}\right)^2 + \left(\frac{\phi_b \Delta T {}^x\text{R}_b}{m_s^2} \sigma_{m_s}\right)^2} \quad (4)$$

For typical RPO fraction CO_2 masses ($\approx 100 \mu\text{g C}$) and ΔT ($\approx 100^{\circ}\text{C}$) encountered during sample analyses, blank carbon correction shifts $\delta^{13}\text{C}$ values by -0.02‰ (for $\delta^{13}\text{C} = -35\text{‰ VPDB}$) to $+0.15\text{‰}$ (for $\delta^{13}\text{C} = +5\text{‰ VPDB}$) and Fm values by -0.002 (for $\text{Fm} = 0.01$) to $+0.002$ (for $\text{Fm} = 1.0$), within the typical analytical uncertainty of these measurements. While

^{14}C content of graphite targets containing as little as $6\ \mu\text{g C}$ has been accurately analyzed at NOSAMS (Shah Walter et al. 2015), we recommend a minimum RPO fraction mass of $25\ \mu\text{g C}$ in order to keep blank carbon corrections below 0.5‰ for $\delta^{13}\text{C}$ and 0.01 for Fm (assuming $\Delta T = 100^\circ\text{C}$). A spreadsheet for performing all blank correction calculations is included in the supplementary material (Table S1).

Isotope Mass Balance

If sample carbon is completely converted to CO_2 by the end of an analysis and is efficiently transferred to the vacuum line, the mass-weighted mean CO_2 isotope composition of blank-corrected RPO fractions should match independently measured bulk values within analytical uncertainty. To test this, we compare RPO mass-weighted mean compositions with bulk measurements for a range of sample types (SRMs, dissolved organic carbon, fluvial/marine total suspended sediments, soils, and lacustrine/marine sediments). Bulk $\delta^{13}\text{C}$ values were obtained either using an elemental analyzer coupled to a continuous-flow IRMS following Whiteside et al. (2011) or on a dual-inlet IRMS after conversion to CO_2 by closed-tube combustion as described in McNichol et al. (1994a). Bulk Fm was measured at NOSAMS following standard preparation methods for each sample type (McNichol et al. 1994b) and uncertainty for each bulk measurement is taken as the measured analytical uncertainty. We calculate RPO mass-weighted mean isotope compositions ($\overline{xR_s}$) following

$$\overline{xR_s} = \sum_{j=1}^n f_j xR_{s,j} \quad (5)$$

where n is the total number of CO_2 fractions collected throughout the analysis, f_j is the contribution of fraction j to the total mass of CO_2 such that $\sum_j f_j \equiv 1.0$, and $xR_{s,j}$ is the blank-corrected $^{x}\text{C}/^{12}\text{C}$ isotope ratio of fraction j . Additionally, assuming that f_j is known perfectly (i.e. since $\sum_j f_j$ must equal 1.0 by definition), we estimate the mass-weighted mean isotope uncertainty according to

$$\sigma_{\overline{xR_s}} \cong \sqrt{\sum_{j=1}^n (f_j \sigma_{xR_{s,j}})^2} \quad (6)$$

To test the ability of RPO mass-weighted mean isotope values to predict measured bulk values, we performed orthogonal distance regression (ODR), including uncertainty in both x and y variables, using the SciPy package in Python v3.5. and a weighting factor for each sample that is inversely proportional to the uncertainty in each measurement (Boggs and Rogers 1990; Oliphant 2007). All data presented here are either taken from the literature (Rosenheim and Galy 2012; Rosenheim et al. 2013a) or are originally presented in this study.

Stable Isotope Mass Balance

On average, the RPO mass-weighted mean isotope composition is depleted in ^{13}C by $(0.8 \pm 0.9)\text{‰}$ relative to bulk measurements ($n = 66$) independent of RPO analytical conditions (Figure 3), as has been described previously (Rosenheim and Galy 2012; Rosenheim et al. 2013a). To test if residual ^{13}C -enriched carbon remaining after RPO analysis could cause this depletion, Rosenheim and Galy (2012) requantified the carbon content of total suspended sediment samples after ramping to 1000°C and determined that only $\approx 0.003\%$ of initial carbon remained. Therefore, for the samples tested therein, Rosenheim and Galy (2012) concluded that low yield could not explain the observed bias. We tested additional potential sources

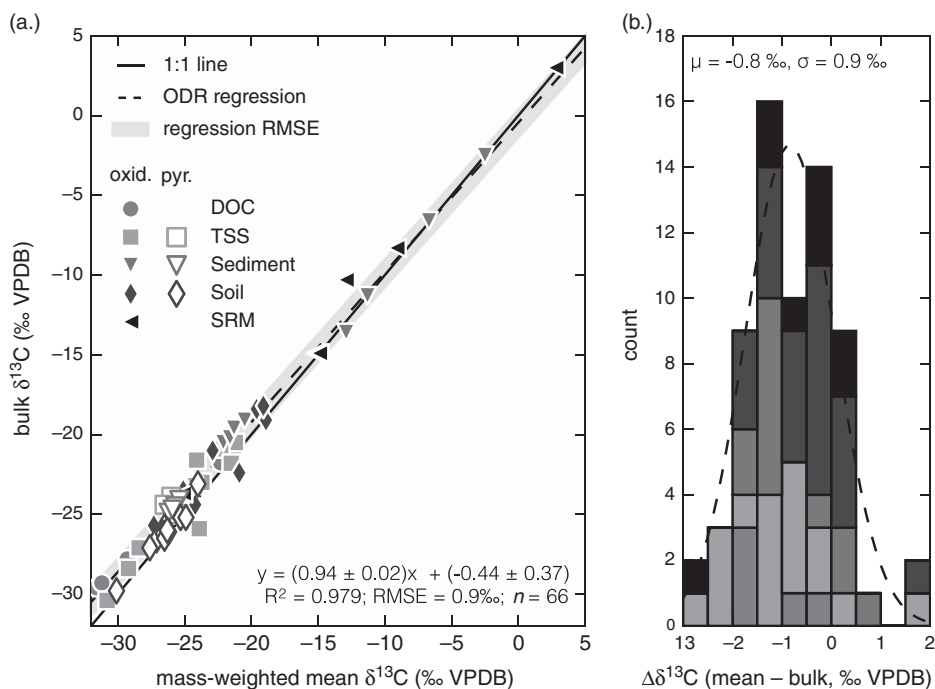


Figure 3 (a.) Cross-plot of RPO mass-weighted mean versus independently measured bulk $\delta^{13}\text{C}$ values for all samples in this study in which $\delta^{13}\text{C}$ data exist and (b.) the same data presented as a histogram of deviations from bulk values ($\Delta\delta^{13}\text{C} = \delta^{13}\text{C}_{\text{mean}} - \delta^{13}\text{C}_{\text{bulk}}$). Sample abbreviations are as follows: DOC, dissolved organic carbon; TSS, total suspended sediments; SRM, standard reference material.

of this depletion by performing a series of experiments using a CO_2 -He calibration gas mixture with known isotope composition [465.5 ppm CO_2 in He, $\delta^{13}\text{C} = (-14.9 \pm 0.04) \text{‰ VPDB}$] as follows:

1. Plumbing calibration gas directly into the toggling traps (bypassing the ovens of the RPO system) over a range of flow rates: 15, 35, and $50 \text{ mL} \times \text{min}^{-1}$;
2. Freezing CO_2 from the calibration gas for a range of integration times for each of the flow rates in experiment (1): 1, 5, and 10 min; and
3. Plumbing calibration gas through an empty, precombusted reactor insert and collecting CO_2 between 150 and 1000°C , toggling every 170°C for a total of 5 fractions (flow rate = $35 \text{ mL} \times \text{min}^{-1}$, ramp rate = $5^\circ\text{C} \times \text{min}^{-1}$).

The results of experiments (1) and (2) reveal that, for all flow rates and integration times, the collected CO_2 $\delta^{13}\text{C}$ value [$-15.0 \pm 0.1 \text{‰ VPDB}$, $n = 9$] is statistically identical to the accepted value, indicating that dynamic cryogenic trapping within the toggling traps imparts no isotope fractionation. Furthermore, oven temperature does not appear to affect ^{13}C composition, as $\delta^{13}\text{C}$ values from all fractions in experiment (3) are statistically identical with a mean value of $(-15.2 \pm 0.04) \text{‰ VPDB}$ ($n = 5$). Although this is 0.3‰ depleted relative to the accepted value, this bias is smaller than that observed in most samples within our sample set (i.e. up to 3‰ , Figure 3b), suggesting that any fractionation imparted during transport through the hot oven alone cannot cause observed ^{13}C depletion.

However, we note that the mass-weighted mean versus bulk $\delta^{13}\text{C}$ difference is more pronounced in decarbonated samples containing exclusively OC (mean–bulk: $\mu = -1.0\text{‰}$; $\pm 1\sigma = 0.9\text{‰}$; $n = 60$) as compared either to samples containing mixtures of carbonate and OC or pure carbonate SRMs (mean–bulk: $\mu = -0.1\text{‰}$; $\pm 1\sigma = 0.5\text{‰}$; $n = 6$). We therefore hypothesize that isotope fractionation during OC degradation within the RPO oven could cause ^{13}C depletion, potentially due to incomplete oxidation to CO_2 while reduced carbon-containing gases are in contact with the catalyst wire (Figure 1a). This mechanism is consistent with the results of experiment (3) indicating a lack of temperature dependence on isotope fractionation. We therefore recommend that $\delta^{13}\text{C}$ values of each RPO fraction j within a particular sample can be fractionation-corrected according to the difference between mass-weighted mean and bulk measurements of that sample

$$\delta^{13}\text{C}_{s,j,\text{corrected}} = \delta^{13}\text{C}_{s,j} + \left(\delta^{13}\text{C}_{\text{bulk}} - \overline{\delta^{13}\text{C}_s} \right) \quad (7)$$

Furthermore, assuming that the covariance between $\delta^{13}\text{C}_{s,j}$ for each fraction j and the mass-weighted mean value ($\overline{\delta^{13}\text{C}_s}$) is small compared to all other variance terms, we propagate uncertainty associated with fractionation correction according to

$$\sigma_{\delta^{13}\text{C}_{s,j,\text{corrected}}} \cong \sqrt{\sigma_{\delta^{13}\text{C}_{s,j}}^2 + \sigma_{\delta^{13}\text{C}_{\text{bulk}}}^2 + \sigma_{\overline{\delta^{13}\text{C}_s}}^2} \quad (8)$$

¹⁴C Mass Balance

In contrast to $\delta^{13}\text{C}$, mass-weighted mean Fm values typically agree with bulk Fm values within analytical uncertainty across all sample types and analytical conditions (mean–bulk: $\mu = 0.005$; $\pm 1\sigma = 0.014$; $n = 36$; Figure 4). This can be easily explained because Fm is by definition corrected for the $^{13}\text{C}/^{12}\text{C}$ ratio as measured on the AMS (Stuiver and Polach 1977; Santos et al. 2007) such that any mass-dependent fractionation occurring in the RPO instrument is accounted for. It is additionally useful to compare relative deviations between bulk and RPO mean values, as ^{14}C content of samples is highly variable. For the samples analyzed here, this equates to an average mean–bulk relative difference of 1.0% with a standard deviation of 3.3% ($n = 36$), independent of absolute ^{14}C content of the sample (Figure 4b). This agreement between the mass-weighted mean Fm and bulk Fm values further precludes the possibility that a significant amount of isotopically unique carbon remains unreacted after ramping to 1000°C, and is strong evidence that ^{14}C mass balance during RPO analysis is robust over the entire range of Fm values found in nature.

Kinetic Fractionation

Finally, we evaluate the kinetic isotope effect (KIE) due to mass-dependent differences in pyrolysis/oxidation rates between each isotope during temperature ramping. If the amplitude of the KIE is significant relative to natural compositional differences, then changes in $\delta^{13}\text{C}$ values between RPO fractions within a single sample can reflect instrumental fractionation rather than differences in carbon source isotope composition. Quantifying fractionation due to the KIE is therefore critical in order to interpret ^{13}C composition as a carbon source tracer. To do so, we measured $\delta^{13}\text{C}$ values of evolved CO_2 from two carbonate SRMs in high-resolution fashion by toggling every $\approx 20^\circ\text{C}$: (1) travertine calcite (IAEA C2; Rozanski et al. 1992), and (2) Icelandic spar [in-house standard; long-term average $\delta^{13}\text{C} = (3.00 \pm 0.03)\text{‰ VPDB}$]. Because carbonates are chemically and isotopically homogenous, any resulting $\delta^{13}\text{C}$ variability should follow a predictable, Rayleigh-like fractionation line that depends only on the difference in activation energy (E) between the decomposition of ^{13}C - and ^{12}C -containing molecules ($^{13-12}\Delta E = ^{13}E - ^{12}E$; Kwart 1982).

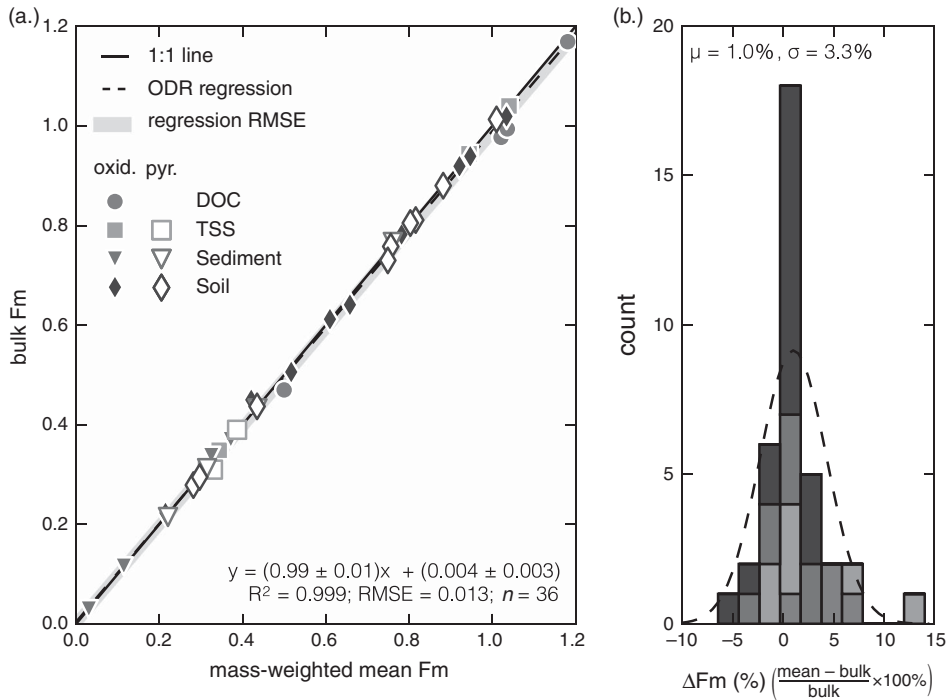


Figure 4 (a.) Cross-plot of RPO mass-weighted mean versus independently measured bulk Fm values for all samples in this study in which Fm data exist and (b.) the same data presented as a histogram of relative deviations from bulk values, in percent $\left[\Delta Fm (\%) = \frac{Fm_{mean} - Fm_{bulk}}{Fm_{bulk}} \times 100\%\right]$. Sample abbreviations are as follows: DOC, dissolved organic carbon; TSS, total suspended sediments.

We describe the carbonate decomposition rate constant at any temperature [$k(T)$] by an Arrhenius equation (here written for ^{12}C)

$$^{12}k(T) = ^{12}k_0 \exp\left(-\frac{^{12}E}{RT}\right) \tag{9}$$

where $^{12}k_0$ is the Arrhenius pre-exponential factor for ^{12}C and R is the ideal gas constant. Following Kwart (1982), the KIE at any temperature [$KIE(T)$] is defined as the ratio of ^{12}C and ^{13}C rate constants at that temperature

$$KIE(T) = \frac{^{12}k(T)}{^{13}k(T)} = \left(\frac{^{12}k_0}{^{13}k_0}\right) \exp\left(\frac{^{13-12}\Delta E}{RT}\right) \tag{10}$$

Equation 10 fundamentally states that, for a given $^{13-12}\Delta E$, $^{12}k_0$, and $^{13}k_0$, $KIE(T)$ decreases with increasing T , indicating that kinetic fractionation within the RPO instrument will be largest for lower temperature components. Furthermore, we can reasonably assume that entropic differences between ^{13}C - and ^{12}C -containing molecules are negligible within the carbonate crystal lattice (c.f. Tang et al. 2000). This assumption implies that $^{12}k(T) = ^{13}k(T)$ as T approaches infinity and requires that $^{12}k_0 = ^{13}k_0 = k_0$ (Cramer 2004). Additionally, for each temperature we compute the ^{13}C composition of the remaining carbonate that has not yet decomposed [$^{13}R_{carb}(T)$] as

$$^{13}R_{carb}(T) = \overline{^{13}R_s} \exp\left(\frac{^{12}I(T) - ^{13}I(T)}{\beta}\right) \tag{11}$$

Table 2 Comparison of k_0 , ^{12}E , and $^{13-12}\Delta E$ values for carbonate SRMs in this study with those calculated using various thermoanalytical techniques on petroleum products.

Sample	Analysis type	k_0 (s ⁻¹)	^{12}E (kJ × mol ⁻¹)	$^{13-12}\Delta E$ (J × mol ⁻¹)	Reference
Travertine (IAEA C2)	RPO (oxidation)	1.0E + 15	326	1.8	This study
Icelandic spar	RPO (oxidation)	1.0E + 15	324	0.3	This study
Tarim Basin kerogen	Sealed pyrolysis	—	218	2–234	Tian et al. (2007)
Tarim Basin crude oil	Sealed pyrolysis	—	230	–52–314	Tian et al. (2007)
Westphalian coal	pyGC-IRMS	2.4E + 14	230–310	30–110	Cramer (2004)
Individual hydrocarbons	Pyrolysis <i>ab initio</i> modeling	—	167–500	15–242	Tang et al. (2000)

where β is the oven ramp rate, $\overline{^{13}R_s}$ is the mass-weighted mean ^{13}C content of the sample calculated by Equation 5, and $^{12}I(T)$ and $^{13}I(T)$ are the temperature integrals for ^{12}C - and ^{13}C -containing molecules according to Braun and Burnham (1987) (here written for ^{12}C)

$$^{12}I(T) \cong \frac{RT^2}{^{12}E} {}^{12}k(T) = \frac{k_0 RT^2}{^{12}E} \exp\left(-\frac{^{12}E}{RT}\right) \quad (12)$$

Finally, following Cramer (2004), we calculate the predicted ^{13}C composition of instantaneously evolved CO_2 at any temperature [$^{13}R_{CO_2}(T)$]

$$^{13}R_{CO_2}(T) = \frac{^{13}R_{carb}(T)}{KIE(T)} = {}^{13}R_{carb}(T) \exp\left(-\frac{^{13-12}\Delta E}{RT}\right) \quad (13)$$

Calculating $^{13}R_{CO_2}(T)$ requires two inputs in addition to $^{13-12}\Delta E$: k_0 and ^{12}E . Here we prescribe k_0 *a priori* and estimate ^{12}E for each SRM by minimizing the root mean squared error (RMSE) between predicted first-order decay rates and observed thermograms using a Nelder-Mead algorithm in the SciPy package for Python v3.5. (Table 2; Nelder and Mead 1965; Oliphant 2007). We note that $^{13}R_{CO_2}(T)$ is insensitive to our choice of k_0 (Dieckmann 2005; White et al. 2011). For example, assuming a large $^{13-12}\Delta E$ value of 100 J × mol⁻¹ for a peak at 700°C, changing k_0 from 10¹⁰ s⁻¹ to 10²⁰ s⁻¹ increases $\delta^{13}C$ of the first 1% of evolved CO_2 by only 1‰ and the first 50% of evolved CO_2 by only 0.2‰. We therefore reasonably choose $k_0 = 10^{15}$ s⁻¹ based on a compilation of literature values [see White et al. (2011) for review]. We then calculate $^{13-12}\Delta E$ that best predicts the ^{13}C composition of all CO_2 fractions for each SRM by minimizing the measured versus predicted RMSE (Nelder and Mead 1965; Oliphant 2007). To accurately compare instantaneous ^{13}C content predicted by Equation 13 to measured RPO fractions (which integrate over time), we use the CO_2 -mass-weighted average temperature for each fraction.

Measured ^{13}C composition for both SRMs is consistent with a $^{13-12}\Delta E$ value between 0.3 and 1.8 J × mol⁻¹ (Table 2; Figure 5), significantly smaller than literature values for petroleum products using various non-isothermal pyrolysis instruments (Table 2). Therefore, for the SRMs analyzed here, predicted CO_2 $\delta^{13}C$ increases by <1‰ until >>99% of initial carbon has been decomposed (Figure 5). However, we note that, on one hand, calculated $^{13-12}\Delta E$ using carbonate SRMs is likely a minimum estimate for environmental samples, as this carbon is already present in a +IV oxidation state, while oxidation of OC could increase $^{13-12}\Delta E$. On the other hand, it has been shown that samples with high molecular diversity—as is expected in environmental OC mixtures—exhibit less *apparent* kinetic isotope fractionation than do single

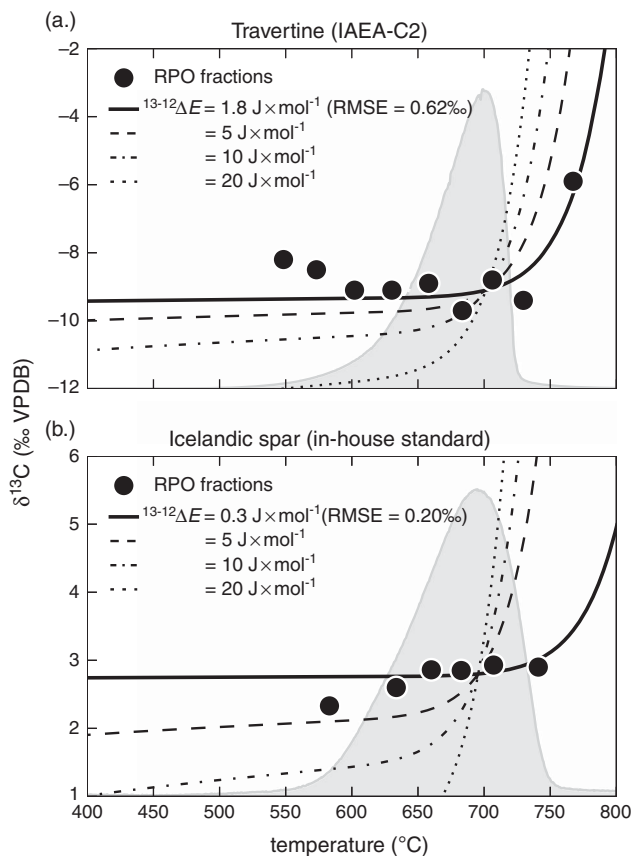


Figure 5 RPO fraction $\delta^{13}\text{C}$ values for two carbonate SRMs [(a.) travertine and (b.) Icelandic spar] plotted with the predicted $\delta^{13}\text{C}$ value at each temperature using best-fit $^{13-12}\Delta E$ values from Equation 13 (solid black line). For reference, predicted $\delta^{13}\text{C}$ values for various $^{13-12}\Delta E$ values are plotted as dashed and dotted lines, while shaded gray regions represent normalized thermograms (unitless). Each RPO fraction is plotted at its CO_2 -mass-weighted mean temperature.

compounds such as the carbonates analyzed here (Cramer 2004). Overall, we recommend that a $^{13-12}\Delta E$ range of $0.3\text{--}1.8 \text{ J} \times \text{mol}^{-1}$ is valid for any component within an RPO analysis, and we consequently predict that kinetic isotope fractionation cannot exceed 1.8‰ during pyrolysis/oxidation of the first 99% of any sample eluting between 150 and 1000°C . In reality, ^{13}C enrichment at $\gg 99\%$ combustion will never be observed during RPO analysis, as each fraction typically contains 10–20% of total carbon. We therefore conclude that $\delta^{13}\text{C}$ variability greater than $1\text{--}2\text{‰}$ between RPO fractions must reflect differences in source carbon isotope composition.

Furthermore, if kinetic fractionation were driving observed ^{13}C variability, $\delta^{13}\text{C}$ values of evolved CO_2 from all samples should increase monotonically with temperature along a trend that depends only on $^{13-12}\Delta E$, which is clearly not observed. Rather, the $\delta^{13}\text{C}$ spread (i.e. max–min) across RPO fractions is highly variable between samples, reaching values as high as 28.8‰ in carbonate-containing lacustrine sediments and as low as 0.3‰

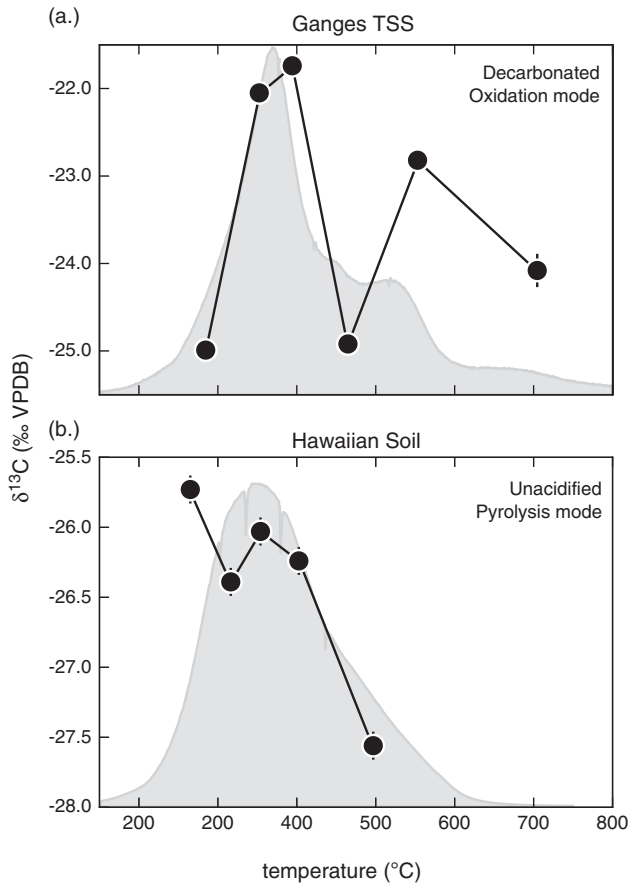


Figure 6 RPO fraction $\delta^{13}\text{C}$ values for two environmental samples: (a.) decarbonated Ganges River TSS (Galy et al. 2008) and (b.) Hawaiian soil (Chadwick et al. 2007). $\delta^{13}\text{C}$ values do not show a monotonic increase with temperature, precluding the possibility that $\delta^{13}\text{C}$ variability in these samples reflects kinetic fractionation. For reference, shaded gray regions represent normalized thermograms (unitless). Each RPO fraction is plotted at its CO_2 -mass-weighted mean temperature.

in decarbonated soils. For three carbonate-containing sediments analyzed here, we additionally measured the $\delta^{13}\text{C}$ value of total inorganic carbon following standard methods (McNichol et al. 1994b) to compare with blank and mass-balance corrected RPO results. For all samples, high-temperature RPO $\delta^{13}\text{C}$ values agree with those of total inorganic carbon within 1‰, further indicating that RPO $\delta^{13}\text{C}$ values accurately reflect source carbon composition.

Lastly, decreasing $\delta^{13}\text{C}$ values have been observed with increasing temperature in select samples such as decarbonated Ganges River total suspended sediments and Hawaiian soils (Figure 6), opposite of trends that would depict kinetic fractionation. Rather, this agrees with the interpretation that labile C_3 OC in these environments is replaced by ^{13}C -enriched, C_4 -derived material (Chadwick et al. 2007; Galy et al. 2008), and is further evidence that measured $\delta^{13}\text{C}$

trends reflect differences in carbon source isotope composition. Combined, the RPO $\delta^{13}\text{C}$ trends from environmental samples analyzed here agree with SRM-based fractionation predictions indicating that kinetic fractionation is small (i.e. less than 1–2‰) in the RPO instrument at NOSAMS.

CONCLUSION

We describe the blank carbon composition, isotope mass balance, and kinetic isotope fractionation within the NOSAMS RPO instrument. Blank carbon mass is significantly smaller than that reported on a similar system (Fernandez et al. 2014) and can be described as a constant flux of $(4.5 \pm 0.7) \text{ ng C} \times \text{°C}^{-1}$ (for a $5\text{°C} \times \text{min}^{-1}$ ramp rate) with an Fm value of 0.555 ± 0.042 and a $\delta^{13}\text{C}$ value of $(-29.0 \pm 0.1) \text{ ‰}$. We find no evidence for significant time-independent blank contribution, likely due to recent valve and plumbing upgrades within the instrument (Plante et al. 2013).

Isotope mass balance on a suite of environmental samples indicates that independently measured bulk Fm is accurately reconstructed using the RPO fraction mass-weighted mean. In contrast, RPO-predicted weighted-average $\delta^{13}\text{C}$ values are slightly depleted relative to measured bulk $\delta^{13}\text{C}$ values, especially for decarbonated samples containing exclusively OC. We eliminate the possibility that this depletion is due to low carbon yield or fractionation within the toggling traps. Rather, we hypothesize that this is caused by incomplete oxidation of reduced gases to CO_2 within the oxidation oven and suggest that $\delta^{13}\text{C}$ of each RPO fraction for a given sample can be mass-balance corrected using the difference between measured bulk and mass-weighted mean values of that sample.

High-resolution $\delta^{13}\text{C}$ measurements on two carbonate SRMs suggest that kinetic isotope fractionation cannot exceed 1.8‰ in the RPO instrument. This agrees with intra-sample $\delta^{13}\text{C}$ trends of the environmental samples analyzed for this study, which display a large range in $\delta^{13}\text{C}$ spread between fractions and are consistent with independently measured carbon source composition. Additionally, selected samples display $\delta^{13}\text{C}$ trends with temperature opposite of that predicted by kinetic fractionation. These results are strong evidence that RPO kinetic fractionation is small and that blank and mass-balance corrected $\delta^{13}\text{C}$ values of each CO_2 fraction reflect carbon source isotope composition to within 1–2‰.

ACKNOWLEDGMENTS

We thank Carl Johnson and the NOSAMS sample-prep lab staff for laboratory assistance. Instrumental improvements to the RPO system were largely the work of Steven Beaupré. Author J D H was partly supported by the NSF Graduate Research Fellowship Program under grant number 2012126152; author V V G was partly supported by the US National Science Foundation (grants OCE-0851015 and OCE-0928582), the WHOI Coastal Ocean Institute (grant 27040213) and an Independent Study Award (grant 27005306) from WHOI; authors G S and P K Z were supported by the WHOI Postdoctoral Scholar Program with funding provided by NOSAMS (OCE-1239667). This manuscript benefited from the constructive comments of two anonymous reviewers and associate editor Dr A J T Jull.

SUPPLEMENTARY MATERIAL

To view supplementary material for this article, please visit <https://doi.org/10.1017/RDC.2017.3>

REFERENCES

- Berner U, Faber E. 1996. Empirical carbon isotope/maturity relationships for gases from algal kerogens and terrigenous organic matter, based on dry, open-system pyrolysis. *Organic Geochemistry* 24(10–11):947–55.
- Bianchi TS, Galy VV, Rosenheim BE, Shields M, Cui X, Van Metre P. 2015. Paleoreconstruction of organic carbon inputs to an oxbow lake in the Mississippi River watershed: Effects of dam construction and land use change on regional inputs. *Geophysical Research Letters* 42:7983–91.
- Boggs PT, Rogers JE. 1990. Orthogonal distance regression. *Contemporary Mathematics* 112: 183–94.
- Braun RL, Burnham AK. 1987. Analysis of chemical reaction kinetics using a distribution of activation energies and simpler models. *Energy & Fuels* 1:153–161.
- Chadwick OA, Kelly EF, Hotchkiss SC, Vitousek PM. 2007. Precontact vegetation and soil nutrient status in the shadow of Kohala Volcano, Hawaii. *Geomorphology* 89:70–83.
- Cramer B. 2004. Methane generation from coal during open system pyrolysis investigated by isotope specific, Gaussian distributed reaction kinetics. *Organic Geochemistry* 35:379–92.
- Currie LA, Kessler JD. 2005. On the isolation of elemental carbon (EC) for micro-molar ^{14}C accelerator mass spectrometry: Development of a hybrid reference material for ^{14}C -EC accuracy assurance, and a critical evaluation of the thermal optical kinetic (TOK) EC isolation procedure. *Atmospheric Physics and Chemistry* 5:2833–45.
- Dieckmann V. 2005. Modelling petroleum formation from heterogeneous source rocks: the influence of frequency factors on activation energy distribution and geological prediction. *Marine and Petroleum Geology* 22:375–90.
- Fernandez A, Santos GM, Williams EK, Pendergraft MA, Vetter L, Rosenheim BE. 2014. Blank corrections for ramped pyrolysis radiocarbon dating of sedimentary and soil organic carbon. *Analytical Chemistry* 86:12085–92.
- Galimov EM. 1988. Sources and mechanisms of formation of gaseous hydrocarbons in sedimentary rocks. *Chemical Geology* 71:77–95.
- Galy VV, France-Lanord C, Lartiges B. 2008. Loading and fate of particulate organic carbon from the Himalaya to the Ganga-Brahmaputra delta. *Geochimica et Cosmochimica Acta* 72:1767–87.
- Kwart H. 1982. Temperature dependence of the primary kinetic hydrogen isotope effect as a mechanistic criterion. *Accounts of Chemical Research* 15:401–8.
- Lopez-Capel E, Abbott GD, Thomas KM, Manning DAC. 2006. Coupling of thermal analysis with quadrupole mass spectrometry and isotope ratio mass spectrometry for simultaneous determination of evolved gases and their carbon isotopic composition. *Journal of Analytical and Applied Pyrolysis* 75:82–9.
- Lopez-Capel E, Krull ES, Bol R, Manning DAC. 2008. Influence of recent vegetation on labile and recalcitrant carbon soil pools in central Queensland, Australia: evidence from thermal analysis-quadrupole mass spectrometry-isotope ratio mass spectrometry. *Rapid Communications in Mass Spectrometry* 22:1751–8.
- McNichol AP, Gagnon AR, Jones GA, Osborne EA. 1992. Illumination of a black box: analysis of gas composition during graphite target preparation. *Radiocarbon* 34(3):321–9.
- McNichol AP, Jones GA, Hutton DL, Gagnon AR. 1994a. The rapid preparation of seawater ΣCO_2 for radiocarbon analysis at the National Ocean Sciences AMS facility. *Radiocarbon* 36(2):237–46.
- McNichol AP, Osborne EA, Gagnon AR, Fry B, Jones GA. 1994b. TIC, TOC, DIC, DOC, PIC, POC—unique aspects in the preparation of oceanographic samples for ^{14}C -AMS. *Nuclear Instruments and Methods in Physics Research B* 92: 162–5.
- Mook WG, van der Plicht J. 1999. Reporting ^{14}C activities and concentrations. *Radiocarbon* 41(3):227–39.
- Nelder JA, Mead R. 1965. A simplex method for function minimization. *The Computer Journal* 7:308–13.
- Oliphant TE. 2007. Python for scientific computing. *Computing in Science Engineering* 9:10–20.
- Pearson A, McNichol AP, Schneider RJ, von Reden KF, Zheng Y. 1998. Microscale AMS ^{14}C measurement at NOSAMS. *Radiocarbon* 40(1):61–75.
- Peters KE. 1986. Guidelines for evaluating petroleum source rock using programmed pyrolysis. *AAPG Bulletin* 70(3):318–29.
- Plante AF, Fernández JM, Leifeld J. 2009. Application of thermal analysis techniques in soil science. *Geoderma* 153:1–10.
- Plante AF, Beupré SR, Roberts ML, Baisden T. 2013. Distribution of radiocarbon ages in soil organic matter by thermal fractionation. *Radiocarbon* 55(2–3):1077–83.
- Reimer PJ, Brown TA, Reimer RW. 2004. Discussion: reporting and calibration of post-bomb ^{14}C data. *Radiocarbon* 46(3):1299–304.
- Rosenheim BE, Galy VV. 2012. Direct measurement of riverine particulate organic carbon age structure. *Geophysical Research Letters* 39:L19703.
- Rosenheim BE, Day MB, Domack E, Schrum H, Benthien A, Hayes JM. 2008. Antarctic sediment chronology by programmed-temperature pyrolysis: methodology and data treatment. *Geochemistry, Geophysics, Geosystems* 9(4):Q04005.
- Rosenheim BE, Domack EW, Santoro JA, Gunter M. 2013a. Improving Antarctic sediment ^{14}C dating using ramped pyrolysis: an example from the Hugo Island Trough. *Radiocarbon* 55(1):115–26.

- Rosenheim BE, Roe KM, Roberts BJ, Kolker AS, Allison MA, Johannesson KH. 2013b. River discharge influences on particulate organic carbon age structure in the Mississippi/Atchafalaya River system. *Global Biogeochemical Cycles* 27:154–66.
- Rozanski K, Stichler W, Gonfiantini R, Scott EM, Beukens RP, Kromer B, van der Plicht J. 1992. The IAEA ^{14}C intercomparison exercise 1990. *Radiocarbon* 34(3):506–19.
- Santos GM, Southon JR, Griffin S, Beaupré SR, Druffel ER. 2007. Ultra small-mass AMS ^{14}C sample preparation and analyses at KCCAMS/UCI Facility. *Nuclear Instruments and Methods in Physics Research B* 259:293–302.
- Schreiner KM, Bianchi TS, Rosenheim BE. 2014. Evidence for permafrost thaw and transport from an Alaskan North Slope watershed. *Geophysical Research Letters* 41:3117–26.
- Shah Walter S, Gagnon AR, Roberts M, McNichol AP, Lardie Gaylord MC, Klein E. 2015. Ultra-small graphitization reactors for ultra-microscale ^{14}C analysis at the National Ocean Sciences Accelerator Mass Spectrometry (NOSAMS) facility. *Radiocarbon* 57(1):109–22.
- Stuiver M, Polach HA. 1977. Discussion: reporting of ^{14}C data. *Radiocarbon* 19(3):355–63.
- Subt C, Fangman KA, Wellner JS, Rosenheim BE. 2016. Sediment chronology in Antarctic deglacial sediments: reconciling organic carbon ^{14}C ages to carbonate ^{14}C ages using Ramped PyrOx. *The Holocene* 26(2):265–73.
- Szidat S, Jenk TM, Gägger HW, Synal HA, Hajdas I, Bonani G, Saurer M. 2004. THEODORE, a two-step heating system for the EC/OC determination of radiocarbon (^{14}C) in the environment. *Nuclear Instruments and Methods in Physics Research B* 223-224:829–36.
- Tang Y, Perry JK, Jenden PD, Schoell M. 2000. Mathematical modeling of stable carbon isotope ratios in natural gases. *Geochimica et Cosmochimica Acta* 64(15):2673–87.
- Tian H, Xiao XM, Wilkins RWT, Li XQ, Gan HJ. 2007. Gas sources of the YN2 gas pool in the Tarim Basin—evidence from gas generation and methane carbon isotope fractionation kinetics of source rocks and crude oils. *Marine and Petroleum Geology* 24:29–41.
- White JE, Catalo WJ, Legendre BL. 2011. Biomass pyrolysis kinetics: a comparative critical review with relevant agricultural residue case studies. *Journal of Analytical and Applied Pyrolysis* 91: 1–33.
- Whiteside JH, Eglinton TI, Olsen PE, Cornet B, McDonald NG, Huber P. 2011. Pangean great lake paleoecology on the cusp of the end-Triassic extinction. *Palaeogeography, Palaeoclimatology, Palaeoecology* 301:1–17.